Surface plasmon resonance biosensor for enzymatic detection of small analytes

2017 Nanotechnology 28 145501

(http://iopscience.iop.org/0957-4484/28/14/145501)

IOP Publishing Nanotechnology
Nanotechnology 28 (2017) 145501 (6pp) https://doi.org/10.1088/1361-6528/aa6284

Surface plasmon resonance biosensor for enzymatic detection of small analytes

Celina Massumi Miyazaki[1], Flávio Makoto Shimizu[2], J R Mejía-Salazar[2], Osvaldo N Oliveira Jr[2] and Marystela Ferreira[1]

[1] Universidade Federal de São Carlos—Campus Sorocaba—São Paulo, Brazil
[2] São Carlos Institute of Physics (IFSC), University of São Paulo (USP), PO Box 369, 13566-590 São Carlos, SP, Brazil

E-mail: marystela@ufscar.br

Received 1 November 2016, revised 10 February 2017
Accepted for publication 23 February 2017
Published 13 March 2017

Abstract

Surface plasmon resonance (SPR) biosensing is based on the detection of small changes in the refractive index on a gold surface modified with molecular recognition materials, thus being mostly limited to detecting large molecules. In this paper, we report on a SPR biosensing platform suitable to detect small molecules by making use of the mediator-type enzyme microperoxidase-11 (MP11) in layer-by-layer films. By depositing a top layer of glucose oxidase or uricase, we were able to detect glucose or uric acid with limits of detection of 3.4 and 0.27 μmol l^{-1}, respectively. Measurable SPR signals could be achieved because of the changes in polarizability of MP11, as it is oxidized upon interaction with the analyte. Confirmation of this hypothesis was obtained with finite difference time domain simulations, which also allowed us to discard the possible effects from film roughness changes observed in atomic force microscopy images. The main advantage of this mediator-type enzyme approach is in the simplicity of the experimental method that does not require an external potential, unlike similar approaches for SPR biosensing of small molecules. The detection limits reported here were achieved without optimizing the film architecture, and therefore the performance can in principle be further enhanced, while the proposed SPR platform may be extended to any system where hydrogen peroxide is generated in enzymatic reactions.

Supplementary material for this article is available online

Keywords: surface plasmon resonance, atomic force microscopy, biosensing

(Some figures may appear in colour only in the online journal)

1. Introduction

Biosensing with surface plasmon resonance (SPR), [1–3] where changes in the local refractive index are converted to an angle (frequency) shift of the resonance, is now widely used for real-time monitoring of adsorption processes and for the study of interactions of biological molecules [4–9]. Because of the need for measurable changes in the refractive index, this technique has been mostly limited to high-molecular weight (large) biomolecules. Attempts to circumvent this limitation have been made by use of competitive assays, [10, 11] molecular imprinting polymers [12] and with electrochemical SPR spectroscopy, [13–16] in which electrochemical reactions are detected around their redox potential in potential scanning experiments. Small molecules can then be detected, but this approach requires a complex experimental setup and control of the electrocatalysis through an external applied potential. Examples of such usage include glucose detection [5] with a system made with osmium-poly (vinylpyridine)-wired horseradish peroxidase and glucose oxidase, with optimized analytical results being achieved by controlling assembly parameters. In a similar application, hydrogen peroxide was detected with a sensor containing a layer-by-layer (LbL) film of graphene and Prussian blue [16].

The limit of detection was 1 μmol l^{-1}, within the range from 5 to 50 μmol l^{-1}, and an external potential of −0.1 V was required for the electrocatalysis to occur.

In order to address the drawbacks in SPR biosensors mentioned above, we developed a mediator type-enzymatic SPR biosensor that is capable of detecting small biomolecules, e.g. glucose and uric acid, even at very low concentrations. This type of biosensor is well known from electrochemistry, where peroxidase can be used as a mediator to reduce H_2O_2 generated by enzymatic oxidation of the substrate, producing a measurable electrical signal [17, 18]. This signal arises from modifying the concentration profile of mobile ions upon changing the redox state of the mediator, [5, 13] which alters its polarizability and refractive index. The main advantage in using this concept for SPR biosensing is that no external potentials need be applied. Here we employed the micro-peroxidase-11 (MP11) as the mediator, whose bioelectrocatalytic activity has been exploited for reduction of H_2O_2 in biosensors [17] and biofuel cells [19]. MP11 consists of amino acid residues 11–21 linked to ferric-protoporphyrin IX through two thioether bonds with the cysteine residues. The sensing unit was produced with the LbL technique, which provides a simple, versatile approach to immobilize biomolecules with preserved activity and that requires a reduced amount of material [20]. To further understand the sensing principle of the proposed system, finite difference time domain (FDTD) simulations of morphology changes were carried out to provide evidence that the mechanism behind biosensing is based on polarizability changes in MP11.

2. Materials and methods

2.1. Experimental

MP11, disodium salt from equine heart cytochrome c, 1925 g mol^{-1}, glucose oxidase (GOx) from *Aspergillus niger*, 100–250 U mg^{-1}, uricase (UOx) from *Bacillus fastidiosus*, 14.5 U mg^{-1}, and poly(ethylene imine) (PEI) were purchased from Sigma-Aldrich and used as received. All reagents were used without further purification. Ultrapure water from a Sartorius arium Lab Water System was used to prepare the saline phosphate buffer (PBS) 10 mmol l^{-1} with 150 mmol l^{-1} NaCl, with which all solutions were made. For the LbL assembly, GOx suspension was obtained in PBS pH 6.3 at 0.2 g l^{-1}. For the UOx suspension, a stock solution was prepared by dissolving it in sodium borate buffer pH 9.0 at 2.0 g l^{-1}. Then, a 1:10 dilution was made in PBS pH 7.4 for final concentration of 0.2 g l^{-1}. PEI and MP11 suspensions were prepared in PBS solutions at 0.5 g l^{-1} and 0.1 g l^{-1} respectively. Each solution has its pH adjusted to 6.3 and 7.4 when working with GOx and UOx systems, respectively.

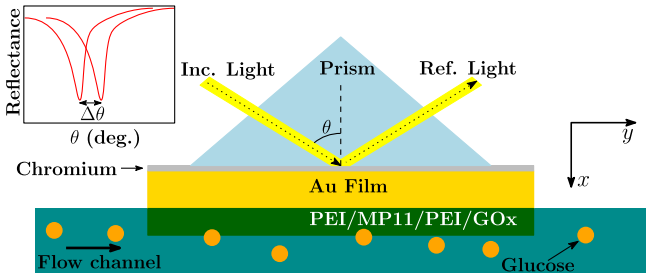

Figure 1. Pictorial representation of the experimental setup.

SPR measurements were made with the BioNavis SPR Navi 200 system, with the sensing device (gold chips) being cleaned in a mixture of $5H_2O$:$1H_2O_2$:$1NH_4OH$ (v/v) for 10 min at 80 °C and washed extensively with ultrapure water. Before use, gold chips were thiol-functionalized by immersion into 150 mmol l^{-1} 11-mercaptopropionic acid ethanolic solution overnight and extensively washed with water and ethanol. The wavelength used was $\lambda = 670$ nm in a Kretschmann [21] configuration, shown schematically in figure 1. The system consists of a prism, $n_p = 1.514$, a $d_{Chr} = 2$ nm chromium adhesion layer with $n_{Chr} = 2.9512 + 2.9584i$, a $d_{Au} = 50$ nm gold metal film with $n_{Au} = 0.1995 + 3.6525i$, and a $d_{Th} = 2$ nm thiol layer with $n_{Th} = 1.442$. Film deposition was performed in flux injecting PEI, MP11 and enzyme solutions at 10 μl min^{-1}. PBS was run after each solution. In the detection experiments a new LbL film was built for each concentration of glucose and uric acid. All sample measurements were performed simultaneously with a reference channel. The morphology of the sensing units was investigated at different steps of the LbL film formation and after the sensing experiments with atomic force microscopy (AFM) in a Bruker Dimension FastScan (Bruker Corp., USA) microscope in the Tapping mode with scan rate of 0.8 Hz.

2.2. Numerical method

The FDTD method is a numerical technique used in computational electrodynamics, and based on the finite difference concept to solve equations in both the time and spatial domains [22, 23]. In this approximation, Maxwell's equations are written in finite differences for the time and spatial derivatives. In this study, excitation of SPRs was performed in the Kretschmann configuration, thus we consider transversal magnetic or *p*-polarized incident light. To numerically simulate the system, we consider the stratification along the *x*-axis, as depicted in figure 1. Thus, we have to solve iteratively the electromagnetic fields $\mathbf{E} = (E_x, E_y, 0)$ and $\mathbf{H} = (0, 0, H_z)$ by using

$$\frac{H_z^{n+1/2}(i,j) - H_z^{n-1/2}(i,j)}{\Delta t} = c\left(\frac{E_x^n(i,j+1/2) - E_x^n(i,j-1/2)}{\Delta x} - \frac{E_y^n(i+1/2,j) - E_x^n(i-1/2,j)}{\Delta x}\right), \quad (1)$$

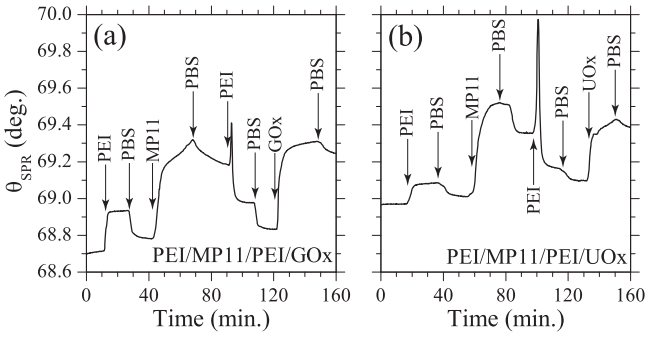

Figure 2. Real-time SPR sensorgrams for LbL deposition of (a) PEI/MP11/PEI/GOx (0.5 g l^{-1} PEI for 15 min, 0.1 g l^{-1} MP11 for 20 min, 0.2 g l^{-1} GOx for 20 min in PBS at pH 6.3) and (b) PEI/MP11/PEI/UOx (0.5 g l^{-1} PEI for 15 min, 0.1 g l^{-1} MP11 for 20 min, 0.2 g l^{-1} UOx for 20 min in PBS at pH 7.4). A flow rate of 15 μl min^{-1} was used during the procedure.

$$\frac{E_x^{n+1}(i, j+1/2) - E_x^n(i, j+1/2)}{\Delta t} = \frac{c}{\varepsilon_{i,j+\frac{1}{2}}}\left(\frac{H_z^{n+1/2}(i, j+1) - H_z^{n+1/2}(i, j)}{\Delta x}\right), \quad (2)$$

$$\frac{E_y^{n+1}(i+1/2, j) - E_y^n(i+1/2, j)}{\Delta t} = \frac{c}{\varepsilon_{i+\frac{1}{2},j}}\left(\frac{H_z^{n+1/2}(i+1, j) - H_z^{n+1/2}(i, j)}{\Delta x}\right), \quad (3)$$

where ε is the relative dielectric permittivity and c is the speed of light in vacuum. The spatial domain is ended along the y-axis by using Bloch periodic boundary conditions, while absorbing perfectly matched layers (PML) were used along the x-axis. The source was taken as a monochromatic plane wave. Numerical results were obtained with the software Lumerical FDTD Solutions, where rough surfaces are directly available to be customized.

3. Results and discussion

Figure 2 shows the sensorgram depicting the immobilization of a polymer and biomolecules using LbL films on the SPR sensor slide. For the LbL film fabrication, a 0.5 g l^{-1} PEI solution was first flowed for 15 min followed by running PBS until stabilization of the signal. A second layer of MP11 was adsorbed for 25 min from a 0.1 g l^{-1} solution followed by PBS flow until stabilization. A further PEI layer was deposited as in the previous one, and finally a GOx (UOx) at 0.2 g l^{-1} was deposited for 20 min and washed with PBS. A flux of 10 μl min^{-1} was used for each step and PBS at pH 6.3 and 7.4 was used for GOx and UOx, respectively. For the PEI/MP11/PEI/GOx film in figure 2(a), the first PEI layer caused a $\Delta\theta = 0.07°$ in the SPR angle, with the shift increasing to $\Delta\theta = 0.4°$ for the next MP11 layer. Upon adsorbing the subsequent PEI layer, the SPR angle shift dropped to $\Delta\theta = 0.12°$ and then raised to $\Delta\theta = 0.51°$ after deposition of the top GOx layer. For the Au/PEI/MP11/PEI/UOx film a similar growth pattern was observed in figure 2(b). The decrease in the SPR angle after injecting PEI following the MP11 layer may suggest material desorption from the sensor surface. However, the AFM images taken for each step of deposition indicated an increased film thickness after PEI layer. This issue will be further discussed when the AFM images are described.

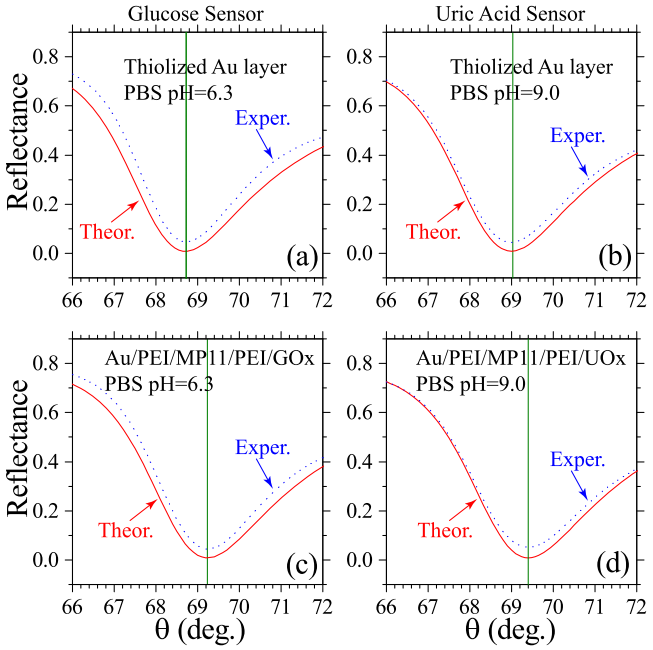

Figure 3. Dotted and solid lines show a comparison of the experimental and numerically fitted θ_{SPR} for the (a) PBS running buffer for the glucose-sensor, (b) PBS running buffer for the uric acid-sensor, and (c) Au/PEI/MP11/PEI/GOx and (d) Au/PEI/MP11/PEI/UOx platforms.

In order to obtain an approximation of the refractive index of the running buffer (RBI), we considered the Au layer as a flat planar surface. The resonant θ_{SPR} value, minimum in the reflection spectrum, was numerically fitted to the experimental values using the FDTD numerical method, with which n_{RBI}= 1.3138 and n_{RBI} = 1.3161 for the glucose-sensor and uric acid-sensor, respectively, as shown in figures 3(a) and (b). An analogous procedure was used to determine the refractive indices for the PEI/MP11/PEI/GOx and Au/PEI/MP11/PEI/UOx platforms in figures 3(c) and (d), leading to n_{GOx} = 1.3181 and n_{UOx} = 1.3194, respectively.

The adsorption of the MP11 layer, necessary for detection, leads to considerable film roughness, as indicated in the AFM images in figure 4 for the PEI/MP11/PEI/GOx SPR platform. The corresponding root mean square (rms) roughness values are given in table 1. The gold sensor covered with PEI presented an rms roughness of 3.49 nm (figure 4(a)), which increases to 153 nm after MP11 deposition (figure 4(b)). The decrease in the SPR angle after the second injection of PEI solution, as already mentioned, may suggest desorption, but in figure 4(c), the maximum height of the PEI/MP11/PEI film is higher than in the step before,

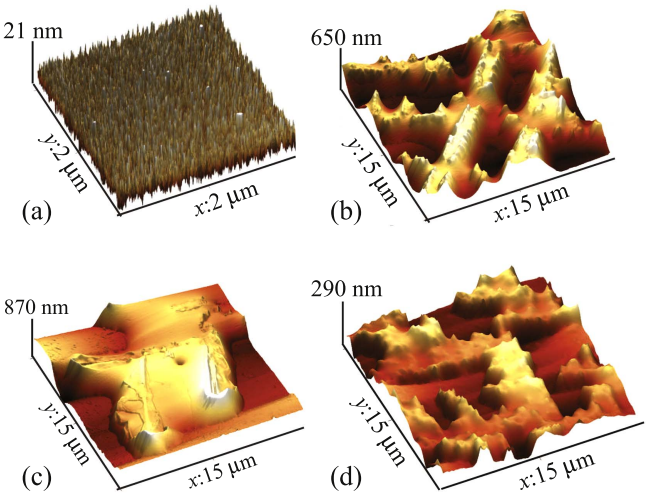

Figure 4. AFM images illustrating the changes in morphology as the PEI/MP11/PEI/GOx LbL film is built. Steps of deposition of (a) PEI, (b) PEI/MP11, (c) PEI/MP11/PEI and (d) PEI/MP11/PEI/GOx on gold sensor.

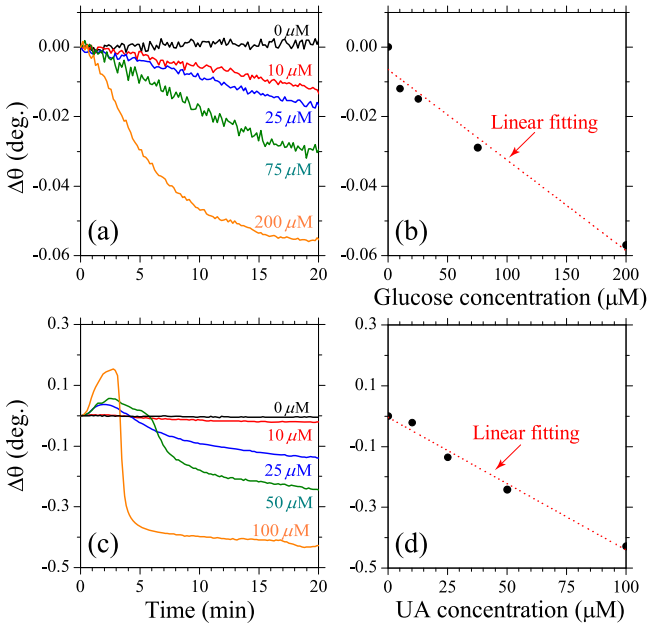

Figure 5. Sensorgrams for glucose (a) and uric acid (c) at different concentrations. The dependence of $\Delta\theta_{SPR}$ on the concentration is shown in (b) for glucose and in (d) for uric acid, where the dashed lines correspond to linear fitting.

Table 1. Root mean square (rms) roughness for each step of the SPR platform growth.

Nanostructure	Rms (nm)
PEI	3.49
PEI/MP11	153
PEI/MP11/PEI	136
PEI/MP11/PEI/GOx	46.6
PEI/MP11/PEI/GOx-Glucose (200 μmol l^{-1})	27

figure 4(b). This confirms deposition of PEI layer, even if there is some loss of material. The rms roughness decreased after consecutive layers following the MP11 layer, probably because deposition of PEI and GOx molecules fills the voids of the highly porous MP11.

The SPR sensing data for glucose and uric acid are shown in figure 5. We injected 100 μl of glucose (uric acid) solutions in PBS with pH 6.3 (PBS with pH 7.4 for uric acid), for different concentrations in flux, and changes in θ_{SPR} were monitored, as shown in figures 5(a) and (c). The sensing mechanism is related to H_2O_2 being generated and reduced by MP11 as glucose is oxidized by GOx, consistent with conclusions from electrochemical experiments [17]. For glucose, this chemical process is described as

$$\beta\text{-D-Glucose} + O_2 \xrightarrow{\text{GOx}} \text{Gluconic acid} + H_2O_2, \quad (4)$$

$$\text{MP-Fe}^{+3} + H_2O_2 \longleftrightarrow [\text{MP-Fe}^{+3} - H_2O_2] \longrightarrow \text{MP}_{Ox1} + H_2O, \quad (5)$$

$$\text{MP}_{Ox1} + e^- + H^+ \longrightarrow \text{MP}_{Ox2}, \quad (6)$$

$$\text{MP}_{Ox2} + e^- + H^+ \longrightarrow \text{MP-Fe}^{+3} + H_2O, \quad (7)$$

where MP_{Ox1} and MP_{Ox2} are intermediate forms of MP11.

In the case of uric acid, it is oxidized according to

$$\text{Uric acid} + O_2 \xrightarrow{\text{UOx}} \text{Allantoin} + H_2O_2, \quad (8)$$

after which the process is again described by equations (4)–(7). In equation (5) MP11 is initially in its reduced form (por-Fe^{+3}), where MP_{Ox1} is produced by heterolytic cleavage of HO–OH in peroxidase/H_2O_2 complex, with a high valent iron-oxoferryl moiety and a π-radical cation on the proto-porphyrin ring (por^{+}-Fe^{IV} = 0 form).

The reasons why the sensing mechanism above yields measurable SPR signals are as follows. Reduction of H_2O_2 by MP11 induces formation of MP_{Ox1}, in accordance with equation (5), as supported by the changes in the UV–vis absorbance spectrum for MP11 in solution (figure S1 in the supporting information, available online at stacks.iop.org/NANO/28/145501/mmedia). Hence, the mobile ions in MP11 are rearranged in the redox state to keep charge neutrality, thus affecting the MP11 polarizability (refractive index). As a consequence the change in SRP angle varied linearly with glucose or uric acid concentration in liquid solutions, as shown in figures 5(b) and (d), respectively. This relationship could be written as

$$\Delta\theta = m \cdot C + b, \quad (9)$$

where m and b are the slope and intercept, respectively. We have found $m = -2.6038 \times 10^{-4}$ and $b = -6.46 \times 10^{-3}$ for glucose (R^2=0.953 88), and $m = -4.36 \times 10^{-3}$ and $b = -4.04 \times 10^{-3}$ for uric acid ($R^2 = 0.980\,21$). The detection limit based on the concentration, corresponding to 3 times the noise response (S/N = 3), was 3.4 μmol l^{-1} for

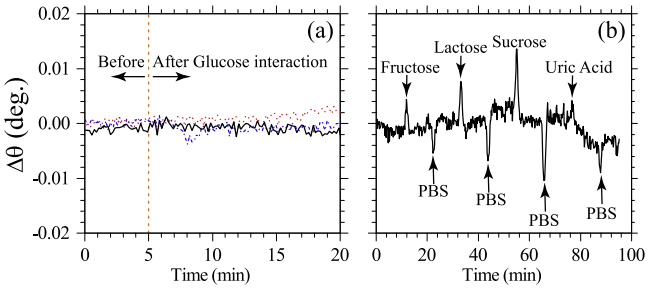

Figure 6. (a) Sensorgram for glucose detection with a Au/PEI/GOx platform. The solid, dotted and dashed–dotted lines correspond to measurements for 500 μmol l^{-1}, 1 mmol l^{-1}, and 10 mmol l^{-1} of glucose. The vertical dashed line is used to separate the process before and after glucose injection in the flow channel. (b) Sensorgram of Au/PEI/MP11/PEI/GOx under injections of 100 μmol l^{-1} of fructose, lactose, sucrose and uric acid.

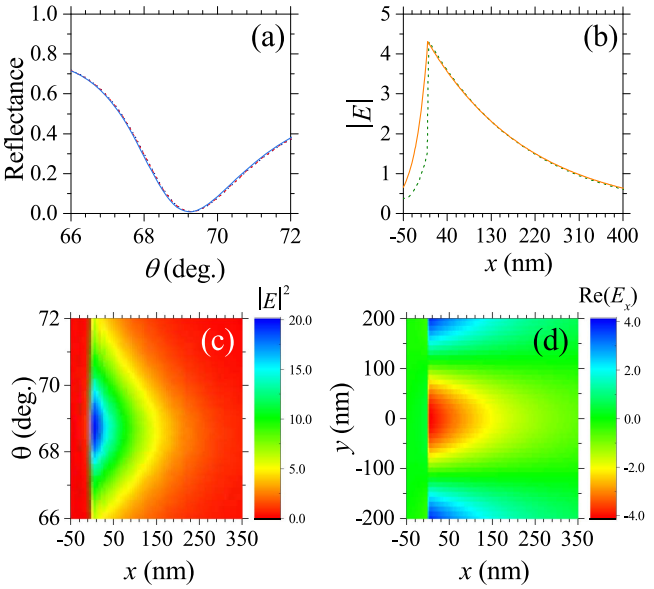

Figure 7. Numerical results for the roughness effects on the PEI/MP11/PEI/GOx SPR biosensing after interaction with 200 μmol l^{-1} of glucose. Dashed and dotted lines in (a) correspond to the rms values 46.6 nm and 27 nm, respectively, while the solid line depicts the results for a perfect planar surface obtained from SMM. (b) Comparison of the E_x evanescent field profiles from the FDTD (with rms = 46.6 nm) and the SPR condition, respectively. (c) and (d) show the corresponding field profiles $|\mathbf{E}|^2$ and Re(E_x), for rms = 46.6 nm, as functions of (x, $y = 0$, θ) and (x, y, $\theta = 69.273°$), respectively.

glucose and 0.27 μmol l^{-1} for uric acid. One should mention that at much higher concentrations the assumption in the simulations of a linear behavior is likely not valid, as some saturation is expected.

It is concluded that the extent of change in MP11 polarizability, as it is oxidized, is responsible for the SPR platforms being able to detect small analytes, even at low concentrations. This we have confirmed with control experiments, in which Au/PEI/GOx and Au/PEI/UOx were built and used for SPR sensing, as shown in figure 6(a). Note that measurable SPR signals could only be obtained in the presence of MP11. Moreover, we evaluated the specificity of the SPR sensing platforms by injecting different carbohydrates and uric acid solutions on the PEI/MP11/PEI/GOx sensor, and negligible non-specific signals were observed in figure 6(b).

Finally, we have also noted that sensing of glucose or uric acid led to large changes in rms roughness of the SPR platforms. For instance, for 200 μmol l^{-1} of glucose (100 μmol l^{-1} of uric acid), the roughness changed from 46.6 to 27 nm (57.2 to 37.5 nm for uric acid). One might have inferred that this change in morphology could be responsible for the sensing, instead of a change in MP11 polarizability. We have ruled out this hypothesis, though, using FDTD simulations, whose results are shown in figure 7. Dashed and dotted lines in figure 7(a) correspond to results with rms = 46.6 and rms = 27 nm, respectively. The solid line is for a flat planar surface, i.e., rms = 0, obtained from the well-known scattering matrix technique [24, 25]. As it can be seen, there are no differences due to roughness or roughness changes. In figure 7(b) we compare the evanescent field $\mathbf{E} = \mathbf{E}_0 e^{-|\mathrm{Im}(k_x)|x}$ from the FDTD calculations (dashed line) with the one from the SPR condition (solid line). Results from SPR condition were obtained by assuming an effective medium below the Au plane, with the corresponding effective refractive index, n_{eff}, calculated by numerically solving the equation $k_{\mathrm{SP}} = k_y$. In figures 7(c) and (d) we show the corresponding field profiles, $\mathbf{E}$ for rms = 46.6 nm, as a function of (x, $y = 0$, θ) and (x, y, $\theta = 69.273°$), respectively, by using the above calculated n_{RBI} and n_{GOx}, where no distortion of profiles due to roughness effects is observed. We assumed 200 nm for the thickness of the PEI/MP11/PEI/GOx platform based on the AFM images in figure 4. This large thickness was not expected owing to the small dimensions of a microperoxidase monomer (1.1 × 1.7 × 3.3 nm). However, microperoxidases are very susceptible to aggregation, forming structures with high molecular mass (>10 kDa). Aggregation via peptide–heme interaction starts at 1 μmol l^{-1}, which has been supported by theoretical [26] and experimental [27] studies. Therefore, we believe that the thickness used is compatible with aggregated microperoxidases transferred onto a solid substrate.

4. Conclusions

We have demonstrated an approach in which mediator-type enzymes are used to improve SPR biosensing. In particular, we developed an indirect mechanism to detect small molecules through the changes in polarizability of MP11, a mediator-type enzyme. The approach is advantageous compared to previous ones because it does not require external potentials. The experiments were performed for uric acid and glucose, but this platform should work with any compound that produces peroxide via enzymatic reactions. It is worth mentioning that low detection limits were already achieved without a systematic search for conditions to optimize sensing performance. Then, one may envisage even higher sensitivity by optimizing SPR platforms where the number of layers in

the LbL films is varied and/or fabricated with other polyelectrolytes under other experimental conditions.

Acknowledgments

This work was supported by the Brazilian Agencies CNPq and FAPESP (2012/15543-7, 2013/14262-7, 2014/17519-1, 2014/15093-7 and 2016/12311-9).

References

[1] Löfås S, Malmqvist M, Rönnberg I, Stenberg E, Liedberg B and Lundström I 1991 Bioanalysis with surface plasmon resonance *Sensors Actuators* B **5** 79–84
[2] Homola J 2008 Surface plasmon resonance sensors for detection of chemical and biological species *Chem. Rev.* **108** 462–93
[3] Daghestani H N and Day B W 2010 Theory and applications of surface plasmon resonance, resonant mirror, resonant waveguide grating, and dual polarization interferometry biosensors *Sensors* **10** 9630–46
[4] Deckert F and Legay F 1999 Development and validation of an immunoreceptor assay for simulect based on surface plasmon resonance *Anal. Biochem.* **274** 81–9
[5] Iwasaki Y, Horiuchi T and Niwa O 2001 Detection of electrochemical enzymatic reactions by surface plasmon resonance measurement *Anal. Chem.* **73** 1595–8
[6] Karlsson R 2004 SPR for molecular interaction analysis: a review of emerging application areas *J. Mol. Recognit.* **17** 151–61
[7] Vutukuru S, Bethi S R and Kane R S 2006 Protein interactions with self-assembled monolayers presenting multimodal ligands: a surface plasmon resonance study *Langmuir* **22** 10152–6
[8] Shankaran D R, Gobi K V and Miura N 2007 Recent advancements in surface plasmon resonance immunosensors for detection of small molecules of biomedical, food and environmental interest *Sensors Actuators* B **121** 158–77
[9] Wang J, Wang F, Chen H, Liu X and Dong S 2008 Electrochemical surface plasmon resonance detection of enzymatic reaction in bilayer lipid membranes *Talanta* **75** 666–70
[10] Carter J A, Triplett E, Striemer C C and Miller B L 2016 A label-free, multiplex competitive assay for small molecule pollutants *Biosens. Bioelectron.* **77** 1–6
[11] Eng L, Nygren-Babol L and Hanning A 2016 Label-enhanced surface plasmon resonance applied to label-free interaction analysis of small molecules and fragments *Anal. Biochem.* **510** 79–87
[12] Yao T, Gu X, Li T, Li J, Zhao Z, Wang J, Qin Y and She Y 2016 Enhancement of surface plasmon resonance signals using a MIP/GNPs/rGO nano-hybrid film for the rapid detection of ractopamine *Biosens. Bioelectron.* **75** 96–100
[13] Koide S, Iwasaki Y, Horiuchi T, Niwa O, Tamiya E and Yokoyama K 2000 A novel biosensor using electrochemical surface plasmon resonance measurements *Chem. Commun.* **2000** 741–2
[14] Gestwicki J E, Hsieh H V and Pitner J B 2001 Using receptor conformational change to detect low molecular weight analytes by surface plasmon resonance *Anal. Chem.* **73** 5732–7
[15] Hu W, Chen S-J, Huang K-T, Hsu J, Chen W, Chang G and Lai K-A 2004 A novel ultrahigh-resolution surface plasmon resonance biosensor with an au nanocluster-embedded dielectric film *Biosens. Bioelectron.* **19** 1465–71
[16] Mao Y, Bao Y, Wang W, Li Z, Li F and Niu L 2011 Layer-by-layer assembled multilayer of graphene/prussian blue toward simultaneous electrochemical and SPR detection of H_2O_2 *Talanta* **85** 2106–12
[17] Graça J S, de Oliveira R F, de Moraes M L and Ferreira M 2014 Amperometric glucose biosensor based on layer-by-layer films of microperoxidase-11 and liposome-encapsulated glucose oxidase *Bioelectrochemistry* **96** 37–42
[18] Castilho T J, Sotomayor M del P T and Kubota L T 2005 Amperometric biosensor based on horseradish peroxidase for biogenic amine determinations in biological samples *J. Pharm. Biomed. Anal.* **37** 785–91
[19] Katz E, Filanovsky B and Willner I 1999 A biofuel cell based on two immiscible solvents and glucose oxidase and microperoxidase-11 monolayer-functionalized electrodes *New J. Chem.* **23** 481–7
[20] Moraes M L, Rodrigues Filho U P, Oliveira O N Jr and Ferreira M 2007 Immobilization of uricase in layer-by-layer films used in amperometric biosensors for uric acid *J. Solid State Electrochem.* **11** 1489–95
[21] Kretschmann E and Raether H 1968 Radiative decay of non radiative surface plasmons excited by light *Z. Naturforsch.* **23a** 2135–6
[22] Sullivan D M 2000 *Electromagnetic Simulation using the FDTD Method* (Piscataway, NJ: IEEE)
[23] Sukhoivanov I A and Guryev I V 2009 *Photonic Crystals: Physics and Practical Modeling* (Berlin: Springer)
[24] Whittaker D M and Culshaw I S 1999 Scattering-matrix treatment of patterned multilayer photonic structures *Phys. Rev.* B **60** 2610–8
[25] Gwon H R and Lee S H 2010 Spectral and angular responses of surface plasmon resonance based on the kretschmann prism configuration *Mater. Trans.* **51** 1150–5
[26] Melchionna S, Barteri M and Ciccotti G 1996 Molecular dynamics of microperoxidases in aqueous and nonaqueous solutions *J. Phys. Chem.* **100** 19241–50
[27] Urry D W 1967 Model systems for interacting heme moieties: I. The heme undecapeptide of cytochrome c *J. Am. Chem. Soc.* **89** 4190–6